SAND2000-0286C

Process Maps for Plasma Spray: Part I: Plasma-Particle Interactions

Delwyn L. Gilmore and Richard A. Neiser
Sandia National Laboratories, Albuquerque, NM

Yuepeng Wan and Sanjay Sampath
State University of New York at Stony Brook, Stony Brook, NY

To be published in the proceedings of ITSC (International Thermal Spray Conference) 2000
ASM International, Materials Park, OH, May 2000

Keywords: air plasma spray, process map, molybdenum, particle diagnostics

DISCLAIMER

Abstract

This is the first paper of a two part series based on an integrated study carried out at Sandia National Laboratories and the State University of New York at Stony Brook. The aim of the study is to develop a more fundamental understanding of plasma-particle interactions, droplet-substrate interactions, deposit formation dynamics and microstructural development as well as final deposit properties. The purpose is to create models that can be used to link processing to performance.

Process maps have been developed for air plasma spray of molybdenum. Experimental work was done to investigate the importance of such spray parameters as gun current, auxiliary gas flow, and powder carrier gas flow. In-flight particle diameters, temperatures, and velocities were measured in various areas of the spray plume. Samples were produced for analysis of microstructures and properties. An empirical model was developed, relating the input parameters to the in-flight particle characteristics. Multi-dimensional numerical simulations of the plasma gas flow field and in-flight particles under different operating conditions were also performed. In addition to the parameters which were experimentally investigated, the effect of particle injection velocity was also considered. The simulation results were found to be in good general agreement with the experimental data.

Introduction

What is a process map? A process map is an integrated set of relationships that link processing to performance. The map can consist of both experimental and computational data. Several types of linking relationships comprise a thermal spray process map. First, how do process conditions affect the particle plume? Experimental studies of this kind have become more common as particle diagnostics technology has improved [1-4]. Also, advances in the power of computational models have led to more theoretical studies of plasma-particle interactions [5-7].

Next, how do the spray particles interact with the substrate to produce the coating microstructure? And last, how does the microstructure behave when tested (i.e., properties and performance), and why? Studies linking particle characteristics to splat formation and coating microstructure and properties have also become more common in recent years [2, 3, 8-10].

Process maps are useful because they allow one to more intelligently control the process in a non-research environment. For example in a production environment, a good process map can enhance stability and reliability while also allowing process modifications to be successfully performed with a minimum of downtime, leading to improved economics. In a research environment, process maps allow one to validate theoretical models. The combination of experimental and theoretical data may allow interpolation and extrapolation to untried conditions. The knowledge gained in the development of a process map can be both fundamental and practical in nature.

In this collaborative study, an effort was made to determine the relationships between spray parameters, in-flight particle characteristics, and deposit microstructures and properties. The focus of this first paper is the link between the processing parameters and the characteristics of particles in the spray plume. The production of samples for microstructural analyses and property measurements will also be described, although the results of those investigations will be detailed in the companion paper which follows.

Experimental Details

Torch set-up. Spraying was performed with a Miller Thermal SG-100 plasma torch in a vertical orientation. The Albuquerque, NM ambient atmospheric pressure for spraying was 83 kPa (12.2 psi). The torch hardware consisted of a 730 anode, a 720 cathode, and a 112 (straight) gas injector ring. The main plasma gas and the powder carrier gas were argon, the auxiliary plasma gas was helium, and the powder carrier gas was argon. Gas flow rates were measured using pressure transducers and jeweled critical orifices calibrated using a primary standard at Sandia. The helium and argon were technical grade. A new anode/cathode set was used, and it was "broken in" prior to data collection by running for 30 minutes at 500 amps, argon only.

A straight powder feed tube with a 3.0 mm inner diameter was used, and powder injection was at 18° forward of normal through a 1.8 mm diameter port. A plasma-densified fine size cut molybdenum powder (Osram Sylvania, #SD152) was used for the work presented in this paper. The volumetrically-weighted powder size distribution as measured by a laser diffraction system (Model LS-100, Coulter Corp., Miami, FL) is given in Table 1.

Table 1. Molybdenum powder size distribution

Vol. Mean (μm)	10% > (μm)	25% > (μm)	50% > (μm)	75% > (μm)	90% > (μm)
28 ± 9	40	35	28	22	16

Particle Diagnostics. Temperature, velocity, and diameter were measured for individual particles in the air plasma spray plume using a DPV-2000 diagnostics system (Tecnar Automation Ltd., St-Hubert, Quebec, Canada). The velocity is determined by time-of-flight between mask slits. The temperature is determined by two-color pyrometry. The diameter is calculated by integration of a pyrometry peak to give the radiated energy for a given particle. This is then used in conjunction with the temperature measurement to give the particle size [11]. The coefficient for the diameter calculations was calibrated by spraying with a different molybdenum powder which had a very narrow size cut. Figure 1 compares the size distribution of the SD152 molybdenum powder before spraying with a typical size distribution for the in-flight particles. The minor differences observed are likely due to slightly differing sensitivities of the two measurement systems.

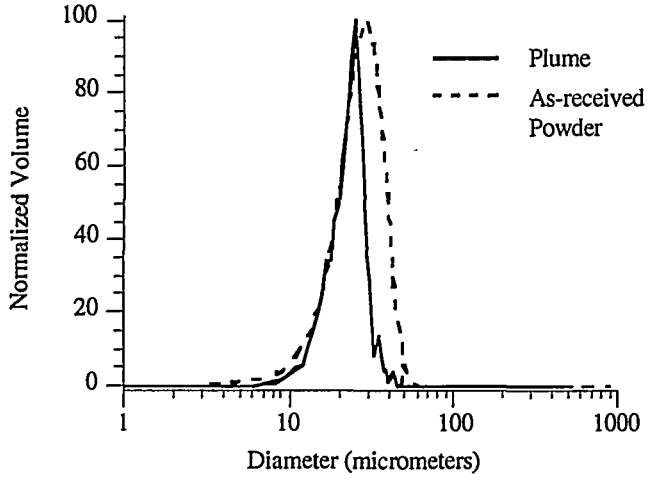

Figure 1. Molybdenum powder size distributions.

Design of Experiments. Based on previous work, it was decided that the plasma torch parameters which would be investigated were current, auxiliary helium flow, and powder carrier gas flow (argon). During the experiments to determine the effects of these parameters on the particle characteristics, the main plasma gas flow was fixed at 50 standard liters per minute (slpm) of argon and the powder feed rate was fixed at 0.18 grams per second (1.5 pounds per hour). A uniform-precision central-composite design was used to construct a 44 point experimental matrix in this 3-dimensional parameter space, including an "outer" three-level full factorial cube (27 points), an "inner" two-level full factorial cube (8 points), and 9 more repetitions of the central point (700 amps, 18 slpm helium, 2 slpm argon powder carrier gas) in order to distinguish the underlying measurement error from lack of fit in later empirical modeling. The parameter values at which particle measurements were collected are given in Table 2.

Table 2. Torch parameters for DoE particle measurements.

	Parameter		
	Current (Amps)	Helium (slpm)	Carrier Gas (slpm)
"Outer cube"	500, 700, 900	12, 18, 24	1.0, 2.0, 3.0
"Inner cube"	580, 820	14.4, 21.6	1.4, 2.6

Particle measurements. Having determined the parameter values at which particle data were to be collected, the order in which measurements were made was randomized. The standoff distance for the diagnostics sensors was fixed at 100 mm downstream of the exit plane of the torch. For each set of torch parameters the sensor-head was then "auto-centered." That is, the sensor was positioned by an automated routine which centered the measurement volume (about 2 mm^3) in the region of maximum particle flow. A map of particle flow in a planar cross-section of the plume is shown in Figure 2. Note that in this figure the central axis of the torch would pass through (0,0), and the powder injection tube would be parallel to the Y-axis at X = 0. Thus, the measurements for this particular run would have been made at a position 6 mm from the central axis of the torch, in line with the powder injection tube (see also Figure 3).

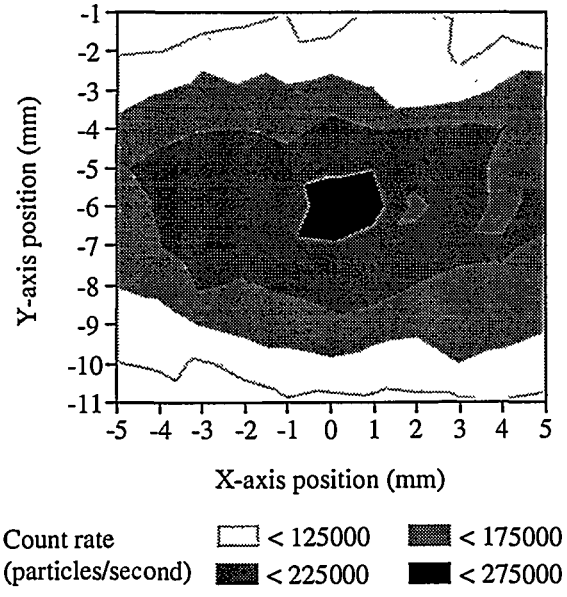

Figure 2. Distribution of particle flow rates within a plume cross-section at 100 mm stand-off. Data collected at "central" conditions (700 A, 18 slpm He, 2.0 slpm carrier gas).

Results and Discussion

Particle data. Before one can begin to address correlations of spray parameters with particle characteristics, one must consider the issue of particle segregation within the plume. If we are to use the mean particle temperatures, velocities, and diameters collected at the point of maximum particle flow, we must be sure that these means are truly representative of the behavior of the plume as a whole. Previous studies have reported conflicting evidence as to the existence of particle segregation in various systems [6, 12-14].

There is evidence of some particle segregation for the spray conditions investigated in this paper, but it was not judged to have a significant influence on the properties of the plume as a whole. Within a 10 mm x 10 mm cross-section centered around the region of maximum flow, mean particle sizes deviated by roughly ± 4 micrometers when measured on a grid of points with 1 mm spacing. This small deviation can be attributed in part to the fact that the standard deviation of the pre-sprayed powder size distribution is only 9 micrometers. The segregation that was observed is in qualitative agreement with simple aerodynamic drag predictions, with the larger particles penetrating farther through the plume than smaller particles, as shown in Figure 3.

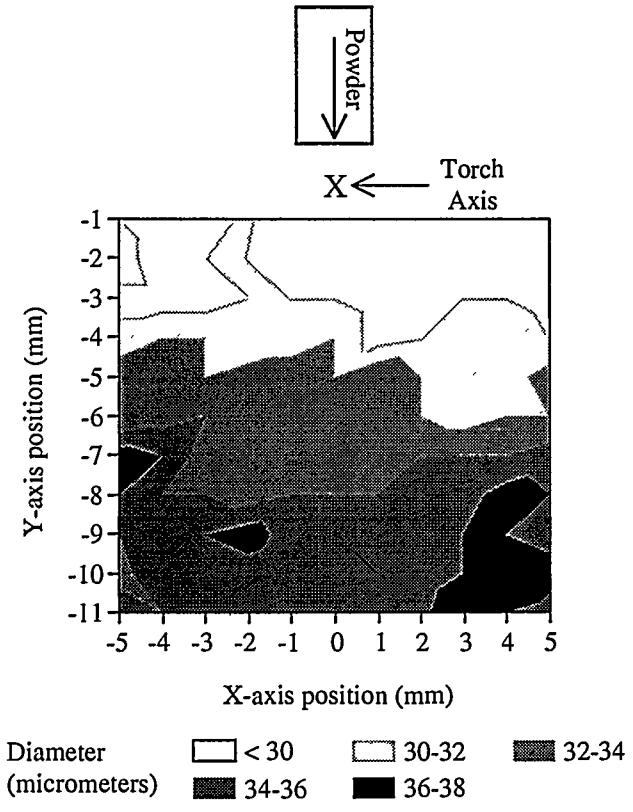

Figure 3. Distribution of particle diameters within a plume cross-section at 100 mm stand-off. Data collected at "central" conditions (700 A, 18 slpm He, 2.0 slpm carrier gas). Spray direction is along Z-axis.

Figure 4 displays particle temperature contours in a plume cross-section sprayed at the "central" conditions of the Design of Experiment. Comparing with Figure 2, it can be seen that the region of hottest particles is shifted only slightly away from the region of maximum flow. From other measurements it was observed that the standard deviation of temperature was approximately 100 °C, so the vast majority of the particles in this central area of the plume appear to be above the melting temperature of molybdenum (2610 °C).

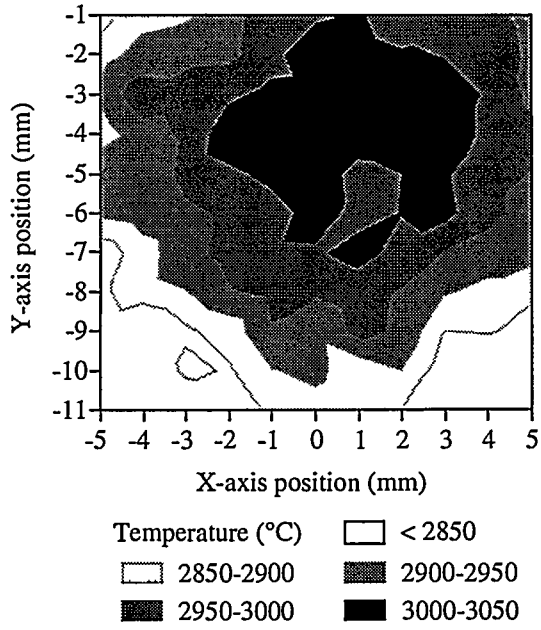

Figure 4. Distribution of particle temperatures within a plume cross-section at 100 mm stand-off and "central" conditions.

A quantitative estimate of the significance, or lack thereof, of particle segregation in the plume has been made by calculating the flow-weighted averages of particle temperature, velocity, and diameter at 121 points throughout the plume (a 10 mm x 10 mm square with 1 mm point spacing). Table 3 shows that the standard deviations of the particle means at these 121 points are no more than 8% of the mean values. That is, although particle segregation exists, it is small, and the largest deviations in particle temperature and velocity occur at the edges of the plume where there are few particles present.

Table 3. Flow-weighted particle statistics for Figs. 2-4.

	Mean ± Std. Dev.	Std. Dev. / Mean
Temperature	2942 ± 69 °C	2.1 %
Velocity	154 ± 11 m/s	7.3 %
Diameter	33 ± 3 μm	8.1 %

Correlations. Figure 5 shows particle data collected at the position of maximum flow for the 35 different spray conditions The mean temperatures and velocities are highly correlated, as might be expected. This makes it more difficult to separate the

effects of particle temperature and velocity on coating microstructure and properties. The mean particle temperature at the position of maximum flow was found to be above the melting point of molybdenum for all spray conditions.

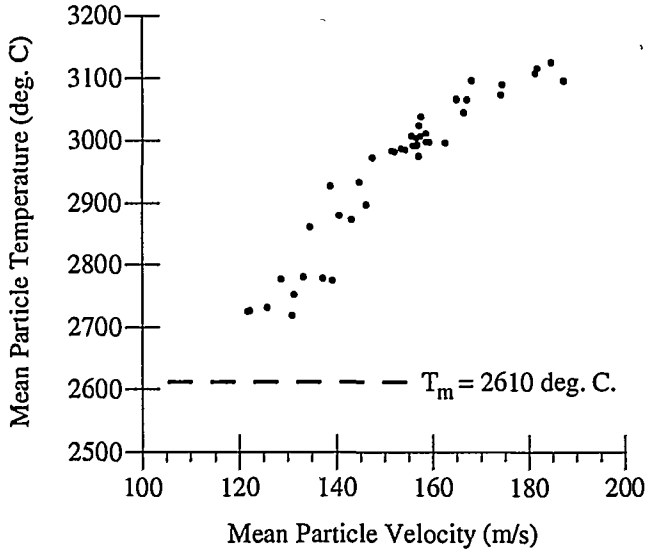

Figure 5. Mean particle temperatures and velocities at the various spray conditions are highly correlated.

Figure 6 shows that, for a given run, particle velocity and diameter were also found to be correlated. The data are fit fairly well by a curve derived from simple aerodynamic drag, with velocity being proportional to the inverse square root of the diameter [15]. There is a significant amount of scatter in the data about this curve, presumably due to the statistical distribution of particle injection trajectories [12].

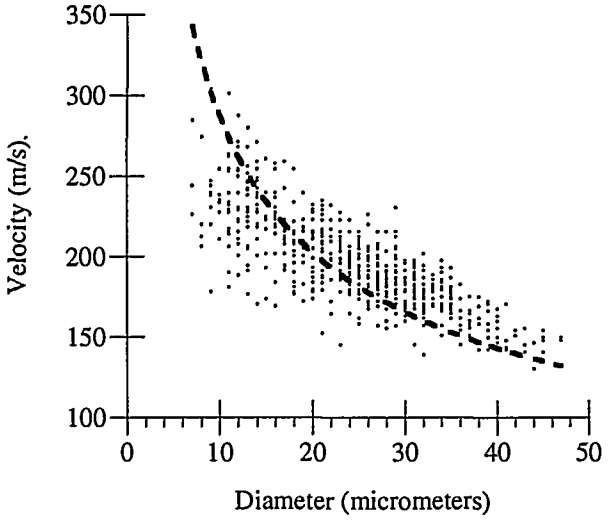

Figure 6. Particle velocities for a given run agree with a simple aerodynamic drag model ($V \propto 1 / d^{1/2}$).

Empirical model. The data from Figure 5 were used to create an empirical model of spray parameter effects on particle temperature and velocity. Mean particle diameter was not significantly affected by the torch parameters (within the ranges investigated). The parameters (current, helium flow, powder carrier gas flow) were first normalized for the ranges investigated, so that the relative importance of each term in the model could be accurately gauged. The particle characteristics were then fit to a quadratic surface in the 3-dimensional parameter space:

$$T_p \text{ or } V_p = C_0 + C_1 * \text{Current} + C_2 * \text{Helium} + C_3 * \text{Carrier gas} + C_4 * \text{Current} * \text{Current} + C_5 * \text{Current} * \text{Helium} + C_6 * \text{Current} * \text{Car. gas} + C_7 * \text{Helium} * \text{Helium} + C_8 * \text{Helium} * \text{Car. gas} + C_9 * \text{Car. gas} * \text{Car. gas} \quad (1)$$

where all parameters are normalized and the coefficients are as given in Figures 7 and 8 below.

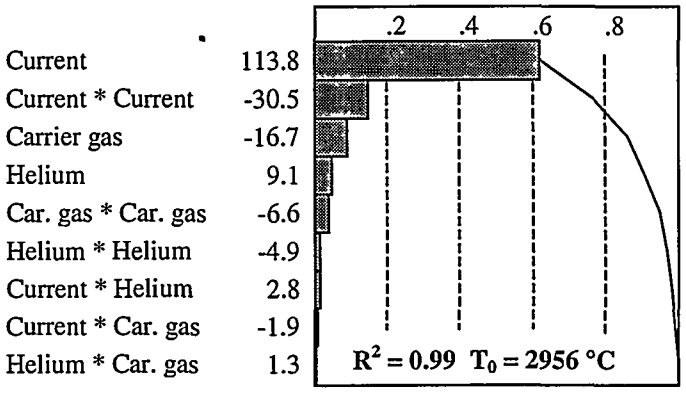

Fig. 7. Pareto plot of parameter effects on particle temperature.

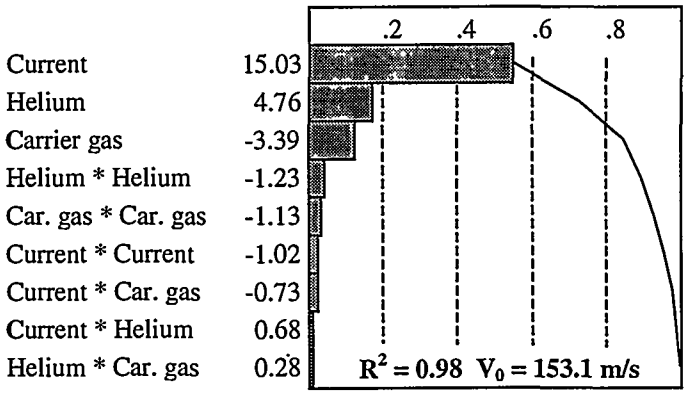

Figure 8. Pareto plot of parameter effects on particle velocity.

For example, referring to Eq. 1 and Figure 7, for spray conditions of 800 amps, 21 slpm helium, and 2.5 slpm powder carrier gas, the model would predict a particle temperature of 2999 °C. All of the parameters in this example would have normalized values of 0.50 (e.g., 800 amps is half-way between

the "central" condition of 700 amps and the highest current used in the DoE, 900 amps).

Relative importance of parameters. Figures 7 and 8 show that the plasma current is the dominant influence on the particle temperature and velocity, as might be expected. In the range of values which were studied, increasing powder carrier gas flow decreased both temperature and velocity, indicating that this system is fairly sensitive to the trajectory of the injected particles. Helium flow has a surprisingly small effect on particle temperature – on average, an increase of 6 slpm only results in a 9 °C rise.

Figure 9 plots the values for particle temperature and velocity predicted from the empirical model given above. Values were calculated at finely spaced intervals over the full range of parameter space investigated: 500 - 900 amps, 12 - 24 slpm helium, 1.0 - 3.0 slpm carrier gas. For comparison, the 44 experimentally measured data points are also shown. As noted previously, temperature and velocity are highly correlated. However, the predicted values show that by properly adjusting the spray parameters, one may vary temperature and velocity independently within small ranges, more so at low values than at high values.

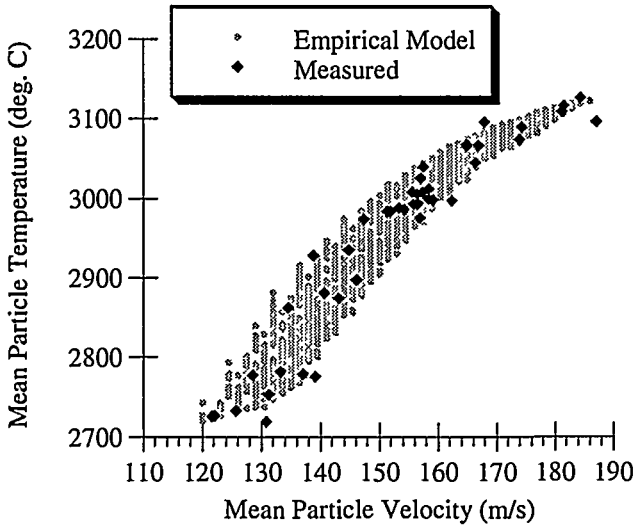

Figure 9. Predicted and measured values for mean particle temperature and velocity.

Test and use of model. In order to evaluate the model, new experimental data were taken at previously untested points in parameter space. Some of these new points were within the limits of the original DoE cube (testing interpolation), and some lay outside those limits (testing extrapolation). The new data points were found to agree with predicted values within 2% on average for absolute temperature, and within 3% on average for velocity. In general, interpolated predictions were found to be more accurate than extrapolated ones, as might be expected.

Production of deposits. Once process maps linking the torch parameters to the particle characteristics were completed, conditions were chosen for the production of samples. These conditions are indicated in Table 4 below. They were selected to produce a range of different microstructures as particle temperatures and velocities were increased. As in the Design of Experiment work, the torch axis was vertical, and the torch-substrate stand-off distance was 100 mm (4.0"). Substrates were mounted eight at a time in a carousel-type fixture, roughly 150 mm (6") in diameter and rotating about a horizontal axis. Thus, a substrate was normal to the torch axis every ⅛ of a revolution.

As substrate temperature has been found to have a large influence on coating microstructures and properties [16, 17], the surface temperature (T_s) of the samples was monitored and controlled by an air-cooling feedback system. This consisted of an infrared pyrometer which measured the temperature of a given substrate (or top surface of the deposit) at a position one-quarter of a revolution after it had passed under the spray plume. This temperature data was then used to control the pressure of the cooling air jet, which was positioned 180° opposite to the torch. With this system it was typically possible to hold a desired temperature within 5 °C. However, the range of substrate temperatures achievable were limited in some cases by the available cooling air flow and the particular heat input for a given set of plasma conditions. Further details of the substrate temperatures at which deposits were produced for subsequent analysis are given in the companion paper which follows.

For a given set of conditions, three types of deposit samples were sprayed: splats (to study the effect of in-flight particle characteristics and substrate temperature on morphology), thin coatings (for wear and residual stress measurements), and thick coatings (for metallography, porosity and thermal conductivity measurements). Splats were produced by passing the torch once over the substrate carousel (rotating at 240 rpm) at a traverse rate of 100 mm/s (4.0"/s) and a powder feed rate of approximately 0.05 grams per second (0.4 pounds per hour). Thin coatings, nominally 100 μm (0.004") thick, were produced by passing the torch over the substrates (150 rpm) about 50 times at a traverse rate of 25 mm/s (1.0"/s) and a powder feed rate of approximately 0.18 grams/sec (1.5 lbs/hr). Thick coatings, nominally 1.3 mm (0.05") thick, were produced with about 250 passes at 7.5 mm/s (0.3"/s), a feed rate of 0.18 grams/sec (1.5 lbs/hr), and a carousel rotational speed of 180 rpm. Particle temperature and velocity were measured for every spray run to insure that they were within the target ranges.

Computational simulations. The LAVA computer code was used to simulate the plasma-particle interactions in the spray plume. A pseudo-three-dimensional model was used, in which particles are modeled in full 3-D space, while the plasma jet is modeled in an axisymmetric 2D domain. Details of this computer model and its algorithms may be found elsewhere [5, 6]. The three different operating conditions selected for the simulations are given in Table 4. The main gas flow was 50 slpm of argon in all 3 cases. Net power was estimated at 68% of current times voltage at the power supply, based on known resistive losses in the cables to the gun and the temperature increase in the gun cooling water flow.

Table 4. Experimental parameters for spraying of deposits

Parameter	Case		
	exp.1c	exp.2b	exp.3a
Current (A)	540	700	860
Voltage (V)	32	35	38
Net Power (kW)	10.2	16.6	22.2
Helium flow (slpm)	12	18	26
Carrier gas flow (slpm)	3.0	2.0	1.0

Particle injection velocity is a major input parameter for the calculation of particle behavior. However, it was not possible to measure the injection velocity in this system, so estimates were calculated based on the known powder carrier gas flow rate and the mean particle size. In order to investigate the effect of injection velocity on the behavior of in-flight particles, simulations were also performed with different injection velocities, indicated as a, b, and c in Table 5.

Table 5. Input parameters used in numerical simulations.

Case	Power (kW)	Particle injection velocity (m/s)	Helium (slpm)
cal.1a	10.2	2.4	12
cal.1b	10.2	4.8	12
cal.1c	10.2	7.1	12
cal.2a	16.6	2.4	18
cal.2b	16.6	4.8	18
cal.2c	16.6	7.1	18
cal.3a	22.2	2.4	26
cal.3b	22.2	4.8	26
cal.3c	22.2	7.1	26

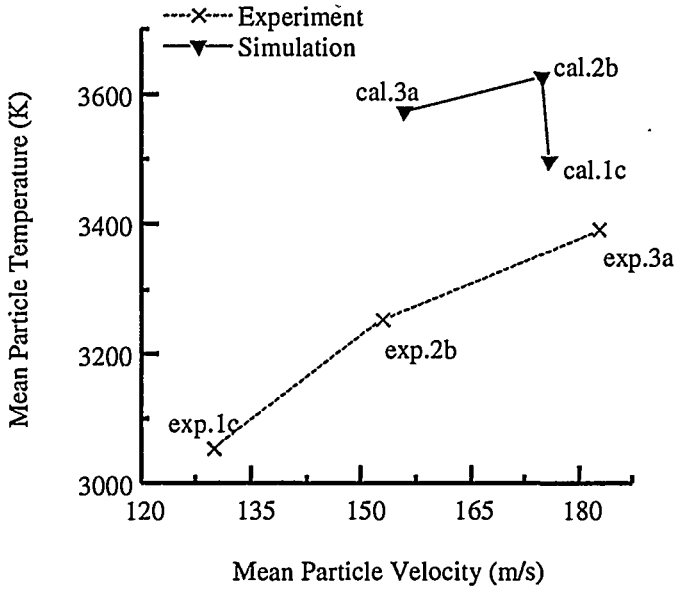

Figure. 10. Computational results for particle injection velocities estimated from carrier gas flow rates.

Figures 10-12 show calculated particle data at a stand-off of 100 mm. Note that the temperatures are given in degrees Kelvin. In Fig. 10, the powder injection velocities for the three calculated cases are different, estimated from the different carrier gas flow rates. The trend exhibited by the experimental data is not observed for the computational results. It is suspected that the estimated injection velocities are not accurate. If the injection velocity is fixed at 4.8 m/s (the middle estimate) for all three cases, the agreement between simulation and experiment is much better, as shown in Figure 11.

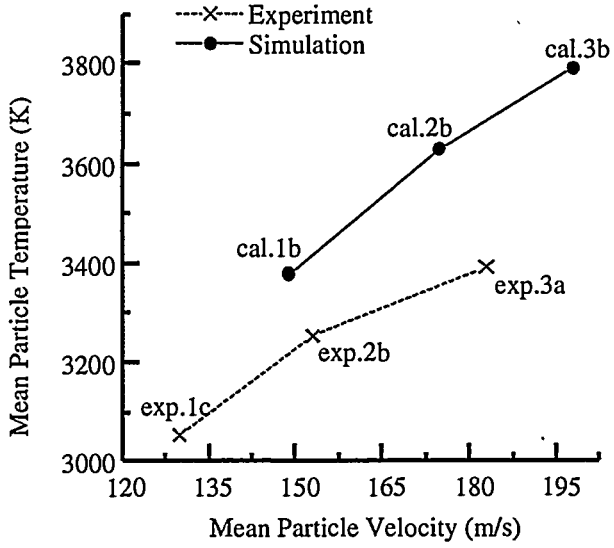

Figure 11. Computational results for constant particle injection velocity.

The effect of particle injection velocity on temperature and velocity is further illustrated in Figure 12, in which calculations performed with different combinations of plasma power level and injection velocity are shown. These calculations indicate that injection velocity can be as important as power in determining the plasma-particle interactions. Therefore, an accurate value of powder injection velocity is critical to the calculation of particle velocity and temperature. It seems likely that the agreement between the experimental and calculated curves in Fig. 11 could be improved by choosing the proper value for the injection velocity.

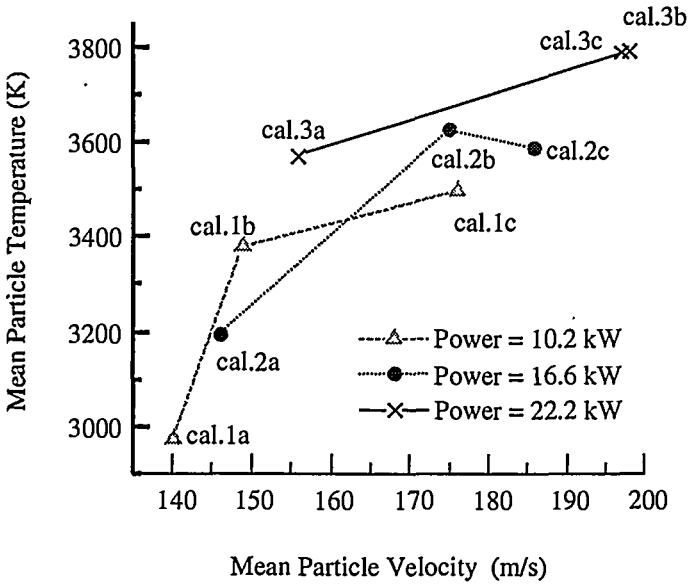

Figure 12. Effect of plasma power and powder injection velocity on in-flight particle temperature and velocity.

Future Work

The eventual goal of this process map work is to understand the relationships between spray parameters, particle characteristics, and coating properties well enough that automated feedback control in real time will be possible. Work has already been done on in-situ measurements of molybdenum coating modulus and stress at various spray conditions. Similar process maps and sets of coatings are being produced for air plasma spray of yttria-stabilized zirconia. This undertaking is somewhat more complex than for molybdenum due to the porous nature of the powder, its higher melting point, and the large thermal gradients which can develop within the in-flight particles.

Conclusions

Diagrams relating torch parameters to the thermal and kinetic energy of sprayed particles can be constructed rapidly. These diagrams can be used to intelligently screen for processing conditions that are likely to produce a wide range of coating microstructures. This screening reduces the need for time-consuming characterization of numerous samples.

In this paper, the air plasma spray of molybdenum was studied. An empirical model was developed from experimental data to link the torch input parameters to the properties of the spray plume. The mean temperature and velocity of the in-flight particles were found to be strongly correlated. Current was found to be the dominant influence on the particle characteristics. A computational model of the plasma-particle interactions verified the observed trends. However, uncertainties as to the particle injection velocity limited the quantitative agreement of the simulations.

Acknowledgments

The authors would like to acknowledge the role of David E. Beatty in the collection of particle data and the production of test samples. Sandia is a multi-program laboratory operated by Sandia Corporation, a Lockheed Martin Company, for the United States Department of Energy under Contract DE-AC04-94AL85000. This work was supported in part by the MRSEC program of the National Science Foundation under award 96-32570.

References

1. J.R. Fincke, W.D. Swank, D.C. Haggard, T.M. Demeny, S.M. Pandit, and A.R. Kashani, *Advances in Thermal Spray Science and Technology (Proc. NTSC '95)*, pp. 117-122, ASM Intl., Materials Park, Ohio (1995)
2. R.N. Wright, J.R. Fincke, W.D. Swank, and D.C. Haggard, *Thermal Spray: Practical Solutions for Engineering Problems (Proc. NTSC '96)*, pp. 511-516, ASM Intl., Materials Park, Ohio (1996)
3. M. Prystay, P. Gougeon, and C. Moreau, *Thermal Spray: Practical Solutions for Engineering Problems (Proc. NTSC '96)*, pp. 517-523, ASM Intl., Materials Park, Ohio (1996)
4. W.D. Swank, J.R. Fincke, D.C. Haggard, S. Sampath, and W. Smith, *Thermal Spray: A United Forum for Scientific and Technological Advances (Proc. UTSC '97)*, pp. 451-458, ASM Intl., Materials Park, Ohio (1997)
5. J.D. Ramshaw and C.H. Chang, *Plasma Chemistry and Plasma Processing*, 12, 299-325 (1993)
6. W.D. Swank, C.H. Chang, J.R. Fincke, and D.C. Haggard, *Thermal Spray: Practical Solutions for Engineering Problems (Proc. NTSC '96)*, pp. 541-546, ASM Intl., Materials Park, Ohio (1996)
7. R.A. Neiser, R.C. Dykhuizen, M.F. Smith, and K.J. Hollis, *Thermal Spray Coatings: Research, Design and Applications (Proc. NTSC '93)*, pp. 61-66, ASM Intl., Materials Park, Ohio (1993)
8. A.C. Léger, M. Vardelle, A. Vardelle, P. Fauchais, S. Sampath, C.C. Berndt, and H. Herman, *Thermal Spray: Practical Solutions for Engineering Problems (Proc. NTSC '96)*, pp. 623-628, ASM Intl., Materials Park, Ohio (1996)
9. S. Sampath, J. Matejicek, C.C. Berndt, H. Herman, A.C. Léger, M. Vardelle, A. Vardelle, and P. Fauchais, *Thermal Spray: Practical Solutions for Engineering Problems (Proc. NTSC '96)*, pp. 629-636, ASM Intl., Materials Park, Ohio (1996)
10. M. Vardelle, P. Fauchais, A. Vardelle, and A.C. Léger, *Thermal Spray: A United Forum for Scientific and Technological Advances (Proc. UTSC '97)*, pp. 535-542, ASM Intl., Materials Park, Ohio (1997)
11. C. Moreau, P. Gougeon, M. Lamontagne, V. Lacasse, G. Vaudreuil, P. Cielo, *Thermal Spray Industrial Applications (Proc. NTSC '94)*, pp.431-437, ASM Intl., Materials Park, Ohio (1994)
12. M. Vardelle, A. Vardelle, and P. Fauchais, J. Thermal Spray Tech., 2, 79-91 (1993)

13. R.A. Neiser and T.J. Roemer, *Thermal Spray: Practical Solutions for Engineering Problems (Proc. NTSC '96)*, pp. 285-293, ASM Intl., Materials Park, Ohio (1996)
14. J.R. Fincke and W.D. Swank, *Thermal Spray: International Advances in Coatings Technology (Proc. ITSC '92)*, pp. 513-518, ASM Intl., Materials Mark, Ohio (1992)
15. R.C. Dykhuizen and M.F. Smith, J. Thermal Spray Tech., 7, 205-212 (1998)
16. A. Haddadi, F. Nardou, A. Grimaud, and P. Fauchais, *Advances in Thermal Spray Science and Technology (Proc. NTSC '95)*, pp. 249-254, ASM Intl., Materials Park, Ohio (1995)
17. J. Matijicek, S. Sampath, and H. Herman, *Thermal Spray: Meeting the Challenges of the 21st Century (Proc. ITSC '98)*, pp. 419-424, ASM Intl., Materials Park, Ohio (1998)